

Original Research

Transcriptome Mapping of the Internal N7-Methylguanosine Methylome in Messenger RNAs in Human Oral Squamous Cell Carcinoma

Minmin Li^{1,2,†}, Ning Song^{1,2,†}, Dongyuan Sun^{1,2,†}, Yang Yu^{1,2}, Wentian Zheng^{1,2}, Xinyue Zhang^{1,2}, Jicheng Ying¹, Rongqi Sun¹, Mengqi Xu¹, Tao Guo^{3,*} , Yingying Jiang^{1,2,*} 

¹School of Stomatology, Weifang Medical University, 261053 Weifang, Shandong, China

²Weifang Key Laboratory of Oral Biomedicine, Weifang Medical University, 261053 Weifang, Shandong, China

³Department of Pathophysiology, School of Basic Medical Sciences, Weifang Medical University, 261053 Weifang, Shandong, China

*Correspondence: guotao@wfmw.edu.cn (Tao Guo); jiangyy@wfmw.edu.cn (Yingying Jiang)

†These authors contributed equally.

Academic Editors: Ilgiz Gareev and Ozal Beylerli

Submitted: 13 July 2023 Revised: 28 August 2023 Accepted: 8 September 2023 Published: 6 December 2023

Abstract

Background: Internal N7-methylguanosine (m7G) methylation in mammalian messenger RNAs (mRNAs) is essential in disease development. However, the status of internally m7G-modified mRNAs in oral squamous cell carcinoma (OSCC) remains poorly understood. **Methods:** Methylated RNA immunoprecipitation sequencing (MeRIP-seq) was used to identify the m7G modification level of mRNAs and the expression of mRNAs between OSCC and normal tissues. These differentially methylated and expressed genes were subjected to Gene Ontology (GO) enrichment, Kyoto Encyclopedia of Genes and Genomes (KEGG) pathway analysis and construction of protein-protein interaction (PPI) networks. Quantitative real-time PCR (qPCR) assay was performed to detect the expression of Baculoviral IAP Repeat Containing 3 (*BIRC3*) *in vitro*. The biological function of *BIRC3* in OSCC was clarified using CCK-8, Transwell migration and Western blot assays. **Results:** The m7G-mRNA profile showed 9514 unique m7G peaks within 7455 genes in OSCC tissues. In addition, the most conserved m7G motif within mRNAs in OSCC was GGARG (R = G/A). The identified m7G peaks were mainly distributed in the coding sequence region within mRNAs in OSCC. GO enrichment and KEGG pathway analyses showed that m7G-modified genes were closely related to cancer progression. m7G-modified hub genes were screened from the constructed PPI networks. Furthermore, *BIRC3* with high m7G methylation showed high expression in OSCC cell lines, as confirmed by qPCR assay. Functionally, the knockdown of *BIRC3* significantly inhibited the proliferation and migration ability of CAL-27 cells *in vitro* functional assays. In addition, the relative expression of E-cadherin expression was elevated, while Vimentin and N-cadherin protein expression was decreased in CAL-27 cells transfected with si-BIRC3. This study suggests that *BIRC3* could promote OSCC proliferation and migration, which may be associated with involvement in epithelial-mesenchymal transition (EMT) progression. **Conclusions:** This paper constructed a transcriptome map of internal m7G in mRNAs, which provides potential research value to study the role of m7G methylation in OSCC.

Keywords: oral squamous cell carcinoma; N7-methylguanosine; messenger RNAs; methylated RNA immunoprecipitation sequencing; bioinformatic analysis; BIRC3

1. Introduction

Oral squamous cell carcinoma (OSCC) is one of the most common malignant tumors worldwide [1]. Recent studies have confirmed that the incidence and mortality rate of OSCC are increasing annually due to the high local recurrence rate and susceptibility to metastasis [2,3]. Although technological advances in surgery, radiotherapy, and chemotherapy have improved the local control of OSCC, the 5-year survival rate of OSCC patients has remained at less than 60% [2,4]. Therefore, exploring the pathogenesis of OSCC and identifying effective therapeutic targets are crucial to improving OSCC patients' prognoses.

RNA methylation is an essential epigenetic modification in post-transcriptional regulation [5]. N7-

methylguanosine (m7G), one of the most common types of RNA methylation, adds a methyl group to the 7th N of RNA guanine in the presence of methyltransferase [6]. Many previous studies have confirmed that m7G methylation is found in ribosomal RNA (rRNA) [7], transfer RNA (tRNA) [8], microRNA (miRNA) [9] and long non-coding RNA (lncRNA) [10] structures. Recently, Zhang *et al.* [11] discovered internal m7G sites within mammalian mRNAs using advanced m7G-methylated RNA immunoprecipitation sequencing (m7G-MeRIP-seq) technology. Furthermore, m7G methylation within mRNAs can affect disease development [12,13]. Specifically, m7G-modified mRNAs can promote angiogenesis in peripheral arterial disease [12]. Internal m7G methylation within mR-



NAs is identified in acute myeloid leukemia (AML) using m7G-MeRIP-seq, and hyper m7G-modified genes are associated with multidrug resistance in AML [13]. Moreover, it has been confirmed that m7G-modified tRNAs can participate in tumor progression in head and neck squamous cell carcinoma (HNSCC) [14,15]. For example, m7G-modified tRNAs can regulate critical signaling pathways (PI3K/AKT/mTOR and WNT/ β -catenin), affecting the progression of HNSCC [14,15]. Many studies have confirmed that N6-methyladenosine (m6A) modifications are common in mRNAs, and can influence cancer progression through regulation of methylation in OSCC [16]. However, the status of internal m7G methylation within mRNAs in OSCC remains poorly understood.

Therefore, to study the role of m7G methylation in OSCC, we aimed to construct and analyze the transcriptome mapping of internal m7G in mRNAs. The comprehensive bioinformatics analysis showed the difference in mRNA m7G methylation and the expression of mRNAs between OSCC and normal tissues. Moreover, Gene Ontology (GO) enrichment, Kyoto Encyclopedia of Genes and Genomes (KEGG) analysis and construction of protein-protein interaction (PPI) networks for m7G-modified genes were performed. Ultimately, the biological functions of the screened m7G-modified Baculoviral IAP Repeat Containing 3 (*BIRC3*) gene in OSCC were clarified *in vitro*. In conclusion, our study analyzed the characteristics and potential functions of these m7G-modified genes, which can provide potential research value to study the role of m7G methylation in OSCC.

2. Methods and Materials

2.1 Tissue Collection, Library Construction and Sequencing

Six tissue samples (C1/N1, C2/N2, and C2/N3) from three OSCC patients were collected from the First Affiliated Hospital of Weifang Medical University. This study was approved by the Ethics Committee of Weifang Medical University [17], and informed consent was obtained from all patients. Library construction and sequencing were performed by CloudSeq Inc. (Shanghai, China), and concrete details about that sequencing procedure have been described in the study [17]. In brief, by using m7G-specific antibodies to enrich the m7G-methylated RNA fragments and combined with high-throughput sequencing technology, m7G methylation on RNA was located and quantified.

2.2 Sequencing Analysis

The raw reads generated were first subjected to Q30 quality control. Then, high-quality clean reads were obtained using cutadapt software (Version: 1.9.3, Berlin, Germany) [18]. The high-quality reads were compared with the reference genome using Hisat2 software (Version: 2.0.4, Baltimore, MD, USA) [19]. Raw counts at the gene level were obtained as mRNA expression profiles using HTSeq

software (Version: 0.9.1, Barcelona, Spain). Finally, fold change ≥ 2 and $p \leq 0.05$ were the criteria used to screen differentially expressed genes between OSCC and normal tissues using edgeR software (Version: 3.16.5, Melbourne, VCP, Australia) [20]. The MACS (Bergisch Gladbach, NRW, Germany) default parameters were used to identify methylated sites, and the p -value of peaks was calculated using the Poisson distribution [21]. DiffReps package was used to identify differentially methylated sites, and p -value was calculated using the negative binomial test [22]. Differentially methylated genes were screened out with default screening criteria of fold change ≥ 2 and $p \leq 0.00001$.

2.3 Bioinformatics Analysis

The RCircos package was used to show the distribution of m7G on chromosomes in OSCC and normal tissues [23]. The motif of methylation peaks was identified using Dreme software (Brisbane, QLD, Australia); the motif with the smallest E value was selected to be the most significant [24].

GO and KEGG analyses were performed using the Database for Annotation, Visualization, and Integrated Discovery (DAVID; <https://david.ncifcrf.gov/>) for differentially expressed genes and differentially m7G-modified genes [25]. GO and KEGG terms with $p \leq 0.05$ were considered statistically significant. In addition, the top 10 terms of GO enrichment and KEGG pathway were shown according to the enrichment score $[-\log_{10}(P)]$. The background gene set used for GO and KEGG analysis was the homo sapiens genome (*HGI9*).

PPI networks were constructed for differentially m7G-modified mRNAs using Search Tool for Retrieval of Interacting Genes/Proteins software (STRING; <https://cn.string-db.org/>) [26]; an interaction score of 0.7 (median confidence) was the standard. In addition, the CytoNCA plugin of Cytoscape software (Version: 3.8.0, Palo Alto, CA, USA) was used to screen hub genes based on betweenness centrality scores [27].

2.4 Online Analysis of Databases for Differentially m7G-modified Genes

Tumor Immune Estimation Resource (TIMER; <https://cistrome.shinyapps.io/timer/>), the University of Alabama at Birmingham Cancer Data Analysis Portal (UALCAN; <https://ualcan.path.uab.edu/>) and Gene Expression Profiling Interactive Analysis (GEPIA; <http://gepia.cancer-pku.cn/>) were used to analyze the expression of the *BIRC3* in tumor tissues [28–30].

2.5 Cell Culture

Five human OSCC cell lines (SCC-9, SCC-25, HN6, HN30, CAL-27) used in this study were obtained from the Shanghai Jiao Tong University School of Medicine, and the Research Resource Identifiers (RRIDs) were listed in previous studies [31–33]. The HN6, HN30, CAL-27 cell

lines were cultured in Dulbecco's modified Eagle's medium (DMEM, GIBCO, NY, USA) with 10% fetal bovine serum (FBS, GIBCO, NY, USA) and 1% penicillin and streptomycin (GIBCO, NY, USA), while the SCC-9 and SCC-25 cell lines were cultured in DMEM/F12 (GIBCO, NY, USA) with 10% FBS and 1% penicillin and streptomycin. Normal control cells were obtained from primary cultures of oral mucosal epithelial cells. Oral mucosal epithelial cells were cultured in keratinocyte serum-free medium (GIBCO, NY, USA) with 0.2 ng/mL of recombinant epidermal growth factor (Thermo Fisher Scientific, Waltham, MA, USA). All cells were maintained at 37 °C in a 5% CO₂ atmosphere and were mycoplasma-free (Mycoplasma PCR Detection Kit, Beyotime, Shanghai, China). The study was carried out in accordance with the guidelines of the Declaration of Helsinki and approved by the Ethics Committee of the Weifang Medical University [17]. All cell lines were authenticated shortly before use by the STR profiling technique, carried out by Shanghai Biowing Applied Biotechnology Co., Ltd.

2.6 Total RNA Extraction and Quantitative Real-Time PCR (qPCR)

Total RNA was extracted from cultured cells using TRIzol reagent. Total RNA was reverse transcribed to cDNA using the PrimeScript RT kit (TaKaRa, Tokyo, Japan). Target genes were amplified using a real-time fluorescent quantitative PCR kit (Life Technologies, Carlsbad, CA, USA). Gene expression was normalized for all samples using β -actin, and the gene expression was quantified by the comparative threshold cycle ($2^{-\Delta\Delta CT}$) method. The primer sequences were as follows: *BIRC3*: F: 5'-TCGCTTGAAAAGACTGGGCT-3', R: 5'-CCCGAGATTAGACTAAGTCCCTT-3'; β -actin: F: 5'-CATGTACGTTGCTATCCAGGC-3', R: 5'-CTCCTTAATGTCACGCACGAT-3' (F: forwards, R: rewards).

2.7 Transfection of Small Interfering RNA (siRNA)

Small interfering RNA (siRNA) was designed and synthesized (Sangon Biotech, Shanghai, China). The targeted sequence of si-BIRC3 was 5'-CAGUUCGUACAUUUCUUUCAT-3'. Transfection was performed using Lipo8000TM (Beyotime, Shanghai, China) according to the manufacturer's instructions, and the knockdown efficiency of *BIRC3* was subsequently verified by qPCR. CAL-27 cells transfected with si-BIRC3 were used for the following functional assays.

2.8 Cell Counting Kit-8 (CCK-8) Assay

CAL-27 cells (1.5×10^3 /well) transfected with si-BIRC3 for 24 h were added to 96-well plates in triplicate; subsequently, cells were incubated in a 37 °C, 5% CO₂ incubator for 2 h with 10 μ L of CCK-8 solution (Dojindo, Kumamoto, Japan). The optical density (OD) at 450 nm

was measured daily for 5 days using a microplate reader (Thermo Fisher Scientific, Waltham, MA, USA).

2.9 Transwell Migration Assay

CAL-27 cells (2.5×10^4 /well) transfected with si-BIRC3 for 24 h were placed in the upper chamber in 150 μ L of serum-free DMEM; 600 μ L of DMEM containing 10% FBS was added to the lower chamber and incubated in an incubator at 37 °C and 5% CO₂ for 24 h. After that, the surface cells at the bottom of the chamber were fixed with 4% paraformaldehyde (Beyotime, Shanghai, China), stained with 0.5% crystal violet (Beyotime, Shanghai, China), and photographed in 5 randomly selected fields under an anatomical microscope (Leica S8APO Stereo Microscope, Leica Microsystems, Wetzlar, Hessen, Germany).

2.10 Western Blot

Western blot analysis was performed as previously described [31]. The primary antibodies included anti-E cadherin (Cat# GB11868; 1:1000; Servicebio, Wuhan, China), anti-N cadherin (Cat# GB11135; 1:1000; Servicebio, Wuhan, China), anti-Vimentin (Cat# GB11192; 1:1000; Servicebio, Wuhan, China) and anti- β -actin (Cat# GB11001; 1:1000; Servicebio, Wuhan, China); HRP Goat anti-rabbit IgG (Cat# BL003A; 1:10,000; Biosharp, Guangzhou, China) was used as the secondary antibody. Immunostrips were visualized with ECLUltra (New Cell and Molecular Biotech, Suzhou, China), and grayscale values were analyzed with ImageJ software (Version 1.46R, National Institutes of Health, Bethesda, MD, USA) after imaging [34].

2.11 Statistical Analysis

SPSS 16.0 (IBM Corp., Armonk, NY, USA) was used for statistical analysis, and GraphPad Prism 7.0 (La Jolla, CA, USA) was used to graph the data. An independent samples *t*-test (two groups) was used to compare the significant differences between the two groups; one-way ANOVA was used to compare multiple groups. The results ($p < 0.05$) were considered statistically significant.

3. Results

3.1 Overview of Internal m7G Methylation within mRNAs in OSCC and Normal Tissues

To clarify the overview of internal m7G methylation within mRNAs in OSCC and normal tissues, we took the intersection of C1, C2, and C3 (Supplementary Fig. 1A,C). Meanwhile, we took the intersection of N1, N2, and N3 (Supplementary Fig. 1B,D). The analysis showed 9514 unique m7G peaks within 7455 genes in OSCC tissues (Fig. 1A,B). Internal m7G methylation features within mRNAs in two groups were further analyzed. The internal m7G peaks within mRNAs in both groups were mainly distributed on chromosome 1 (chr1), followed by chromosome 19 (chr19) (Fig. 1C). Furthermore, the distribution of m7G

methylation on all chromosomes in two groups was shown using the RCircos package (Fig. 1D). In addition, the percentage of genes with more than four m7G peaks within mRNAs was found to be 34.54% in OSCC tissues, indicating that internal m7G methylation sites are not unique (Fig. 1E).

3.2 Analysis of the Regional Distribution of Internal m7G Peaks in OSCC and Normal Tissues

Identification of the regional distribution of m7G methylation showed that m7G methylation occurred in all regions within mRNAs, including coding sequence (CDS), 3'untranslated region (UTR), 5'UTR, Start C and Stop C in OSCC tissues and normal tissues (Fig. 1F,H). In OSCC tissues, the proportion of m7G methylation sites distributed in the 5'UTR region was 15.58%. Meanwhile, in normal tissues, the proportion of m7G methylation sites distributed in the 5'UTR region was 14.60% (Fig. 1F). By analyzing the data on the distribution of m7G methylation sites in the mRNA region in the samples (C1, C2, C3, N1, N2, N3), the results showed that there was no difference in the distribution of m7G methylation sites in all mRNA region in the OSCC tissues compared with the normal tissues (Fig. 1G).

3.3 Analysis of Internal m7G Motifs within mRNAs in OSCC and Normal Tissues

The motif sequences were analyzed using Dreme software in OSCC and normal tissues. Notably, GGARG (R = G/A) sequences were highly clustered at the m7G sites (E value of cancer: 7.0×10^{-12} ; E value of normal: 3.8×10^{-6}) in OSCC and normal tissues (Fig. 1I).

3.4 Potential Biological Functions of Differentially Methylated Genes in OSCC

Differentially methylated genes (fold change ≥ 2 , $p \leq 0.00001$) were identified in OSCC tissues using MeRIP-seq. The top 10 hypermethylated genes were listed according to the fold change (Table 1).

To clarify the biological functions of differentially methylated genes in OSCC, GO analysis based on biological processes (BP), cellular components (CC), molecular functions (MF) and KEGG enrichment analysis for these genes were performed. Hyper m7G-modified genes in OSCC were associated with ion transport, multicellular organismal process and transmembrane transport (GO term: BP); an integral component of the plasma membrane, an intrinsic component of the membrane, and cell projection (GO term: CC); transmembrane transporter activity, and ion transmembrane transporter activity (GO term: MF) (Fig. 2A). In contrast, hypo m7G-modified genes in OSCC were related to localization, regulation of signaling and cell communication (GO term: BP); the cytoplasm, intracellular organelle, and the cytosol (GO term: CC); protein binding, enzyme binding, and cytoskeletal protein binding (GO term: MF) (Fig. 2C). Moreover, KEGG pathway analysis

showed that hyper m7G-modified in OSCC were enriched in the calcium signaling pathway and ATP-binding cassette (ABC) transporters (Fig. 2B). In contrast, hypo m7G-modified genes in OSCC were associated with the Hippo and adenosine 5 monophosphate (AMP)-activated protein kinase (AMPK) signaling pathway (Fig. 2D).

3.5 Functional Analysis of Differentially Expressed Genes in OSCC

The heatmap showed gene expression profiles identified by transcriptome sequencing (Supplementary Fig. 2). Volcano and scatter plots showed 2185 upregulated genes and 2022 downregulated genes in OSCC tissues (fold change ≥ 2 and $p \leq 0.05$) (Fig. 3A,B). To investigate the role of differentially expressed genes in OSCC, GO and KEGG pathway enrichment analyses of these genes were performed. Upregulated genes in OSCC were closely associated with response to stress, the cell cycle, and the immune system process (GO term: BP); the cytoplasm, extracellular exosome, and nucleoplasm (GO term: CC); protein, DNA replication origin and ATP binding (GO term: MF) (Fig. 3C). In contrast, downregulated genes in OSCC were related to a muscle system process, muscle contraction, and muscle structure development (GO term: BP); contractile fibers, myofibrils, and sarcomeres (GO term: CC); cytoskeletal protein binding, actin binding, and structural constituent of muscle (GO term: MF) (Fig. 3E). Furthermore, KEGG pathway analysis revealed that upregulated genes in OSCC were involved in the p53 signaling pathway and cell cycle (Fig. 3D). In contrast, downregulated genes in OSCC were associated with cGMP-PKG and the calcium signaling pathway (Fig. 3F).

3.6 Combined Analysis of Differentially Methylated Genes and Differentially Expressed Genes in OSCC

To investigate the biological role of differentially expressed genes affected by m7G methylation in OSCC, the combined analysis were completed. The result showed 1221 genes with upregulated mRNA expression with m7G hypermethylation sites (referred to as hyper-upregulated genes) and 1645 genes of downregulated mRNA levels with m7G hypomethylation sites (referred to as hypo-downregulated genes; fold change ≥ 2 , $p \leq 0.00001$). The top 10 hyper-upregulated genes were shown in Table 2. In addition, GO and KEGG pathway analyses were performed on these genes. GO analysis revealed that the hyper-upregulated genes in OSCC were mostly involved in the mitotic cell cycle, apoptotic process, and cell junction (Fig. 4A); KEGG pathway analysis showed these genes were enriched in the cell cycle, cellular senescence and DNA replication (Fig. 4B). In contrast, GO analysis showed that hypo-downregulated genes in OSCC were involved in muscle contraction, stress fiber, and actin-binding (Fig. 4C); KEGG pathway analysis showed that these genes were enriched in the calcium, apelin, and cGMP-PKG signaling pathways (Fig. 4D).

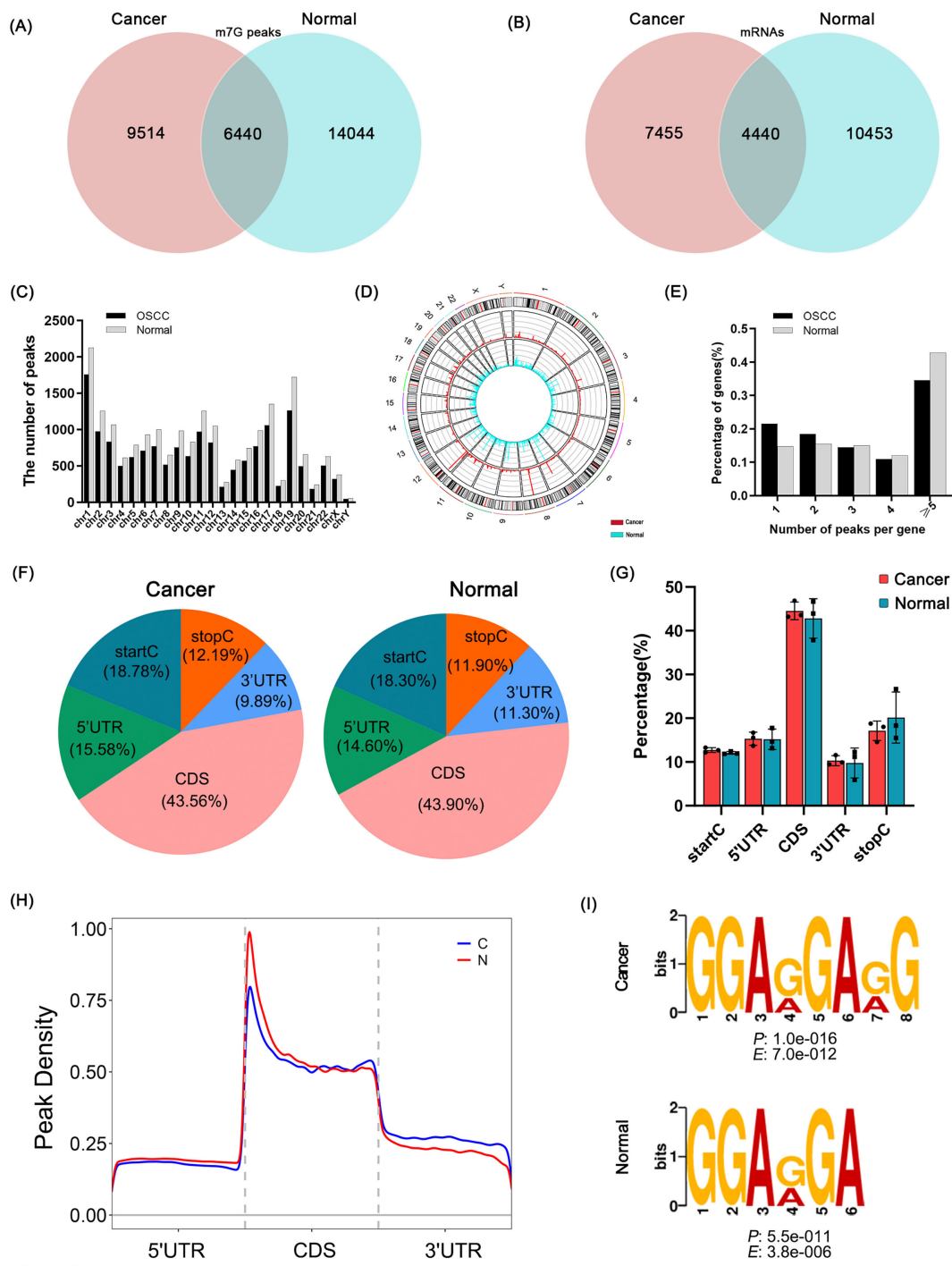


Fig. 1. Overview of internal m7G methylation within mRNAs in oral squamous cell carcinoma (OSCC). (A) Venn diagram showed the unique m7G peaks in OSCC and normal tissues. (B) Venn diagram showed the specific m7G-modified genes in OSCC and normal tissues. (C) Chromosome distribution characteristics of m7G peaks in OSCC and normal tissues. (D) The distribution of m7G at the chromosome was displayed using the Rcirco package in OSCC and normal tissues. (Red: cancer; Blue: normal). (E) The percentage of genes with different m7G peaks in OSCC and normal tissues. (F) Regional distribution of internal m7G methylation sites within mRNAs in OSCC and normal tissues. (CDS, coding sequence; UTR, untranslated region). (G) The bar plot showed the distribution percentage of m7G methylation sites in the mRNA region in the samples (C1, C2, C3, N1, N2, N3). (H) m7G peaks density analysis of m7G methylation in OSCC and normal tissues. (C, cancer; N, normal). (I) The most conserved m7G motifs in OSCC and normal tissues, respectively.

Table 1. The top 10 hypermethylated genes.

Gene name	txStart	txEnd	Chrom	Regulation	log (FC)	<i>p</i>
<i>PPP1R26</i>	138380721	138380739	chr9	Hyper	3.227	3.57×10^{-9}
<i>BIRC3</i>	102208521	102208840	chr11	Hyper	3.062	3.96×10^{-9}
<i>C11orf70</i>	101953801	101953820	chr11	Hyper	3.022	4.05×10^{-9}
<i>SCUBE3</i>	35218901	35219240	chr6	Hyper	2.966	3.45×10^{-9}
<i>KCNA6</i>	4921301	4921720	chr12	Hyper	2.946	3.6×10^{-9}
<i>MLNR</i>	49796321	49796513	chr13	Hyper	2.913	1.25×10^{-8}
<i>CDC42SE2</i>	130727061	130727460	chr5	Hyper	2.903	7.3×10^{-9}
<i>ABCG4</i>	119027581	119027724	chr11	Hyper	2.894	1.32×10^{-8}
<i>ACACB</i>	109666641	109666666	chr12	Hyper	2.884	3.72×10^{-9}
<i>MYH3</i>	10531842	10531940	chr17	Hyper	2.882	1.06×10^{-8}

Table 2. The top 10 hypermethylated-upregulated genes.

Gene Name	chrom	txStart	txEnd	Pattern	m7G change		mRNA change	
					log (FC)	<i>p</i>	log (FC)	<i>p</i>
<i>BIRC3</i>	chr11	102208521	102208840	Hyper-up	3.062	3.96×10^{-9}	2.066	6.49×10^{-4}
<i>FER1L6</i>	chr8	125035683	125035836	Hyper-up	2.858	3.52×10^{-9}	3.817	3.81×10^{-2}
<i>ARHGAP23</i>	chr17	36635676	36635738	Hyper-up	2.786	4.61×10^{-9}	1.137	3.90×10^{-2}
<i>FBXO39</i>	chr17	6690761	6690965	Hyper-up	2.78	3.98×10^{-9}	4.806	3.86×10^{-3}
<i>ECT2</i>	chr3	24582476	24582574	Hyper-up	2.782	8.02×10^{-9}	3.354	1.22×10^{-5}
<i>KIAA0319</i>	chr6	179071101	179071480	Hyper-up	2.747	3.21×10^{-9}	4.404	7.56×10^{-4}
<i>ABL2</i>	chr1	50616781	50616831	Hyper-up	2.744	7.34×10^{-9}	1.433	1.29×10^{-2}
<i>PANX2</i>	chr22	11302081	11302395	Hyper-up	2.742	1.86×10^{-9}	4.93	7.39×10^{-3}
<i>FAM167A</i>	chr8	172534480	172534500	Hyper-up	2.737	5.99×10^{-9}	5.948	1.09×10^{-3}
<i>MMP10</i>	chr11	102641232	102641240	Hyper-up	2.721	3.78×10^{-9}	5.555	1.20×10^{-12}

To explore the protein interactions of differentially expressed methylation genes, PPI networks of these genes were generated using the STRING software. Among these 1221 hyper-upregulated genes, 792 nodes and 440 edges ($p: 1.0 \times 10^{-16}$) were found (Fig. 4E). Among these 1645 hypo-downregulated genes, 1070 nodes and 482 edges were found ($p: 1.0 \times 10^{-16}$) (Fig. 4F). In addition, hub genes were filtered based on intergenic centrality scores using the CytoNCA plugin of Cytoscape software. The top three core genes screened were *TP73*, *CASP1*, and *RUNX3* in the hyper-upregulated genes and *ACTN2*, *PPKACA*, and *MEF2C* in hypo-downregulated genes (Fig. 4E,F).

3.7 Bioinformatic Characteristics and Biological Behavior of the m7G-modified Gene *BIRC3* in OSCC Tissues

By the co-analysis, the heatmap showed the top 10 upregulated genes with high m7G methylation based on fold change (Fig. 5A). The result showed that the highly expressed *BIRC3* gene had the highest m7G methylated peaks (logFC: 3.062) among the top 10 screened genes. The m7G peaks were visualized by Integrative Genomics Viewer software (IGV, Version: 2.14.1, Cambridge, MA, USA), and the *BIRC3* transcript has higher m7G methylation peaks at the sites (chr11: 102208521-102208840) in OSCC tissues than in normal tissues (Fig. 5B). The STRING software showed that the *BIRC3* protein could interact with TNF receptor-associated factor (Fig. 5C).

Furthermore, UALCAN (Fig. 5D), TIMER and GEPIA (Supplementary Fig. 3A,B) showed that *BIRC3* was highly expressed in HNSCC tissues. Then, the expression of *BIRC3* was upregulated in OSCC cell lines (SCC-9, SCC-25, HN6, HN30, and CAL-27), as confirmed by qPCR assay (Fig. 5E). To further investigate the biological function of *BIRC3* in OSCC, CAL-27 cells transfected with si-*BIRC3* were constructed. The *BIRC3* expression in CAL-27 cells was knocked down by the qPCR assay (Fig. 5F). Functionally, the migration of CAL-27 cells transfected with si-*BIRC3* was significantly inhibited in the Transwell migration assay (Fig. 5G). The proliferation of CAL-27 cells transfected with si-*BIRC3* was significantly decreased, as determined by the CCK-8 assay (Fig. 5H). The relative expression of (epithelial-mesenchymal transition, EMT)-related marker protein E-cadherin was significantly increased in the CAL-27 cells transfected with si-*BIRC3*. In contrast, the expression of N-cadherin and Vimentin proteins was significantly decreased in the Western blot assay (Fig. 5I). These results suggest that the knock-down of *BIRC3* could inhibit the biological behavior of OSCC *in vitro*, which may be related to the process of EMT.

4. Discussion

m7G methylation is a common RNA modification that can affect tumor progression, recurrence, and metastasis

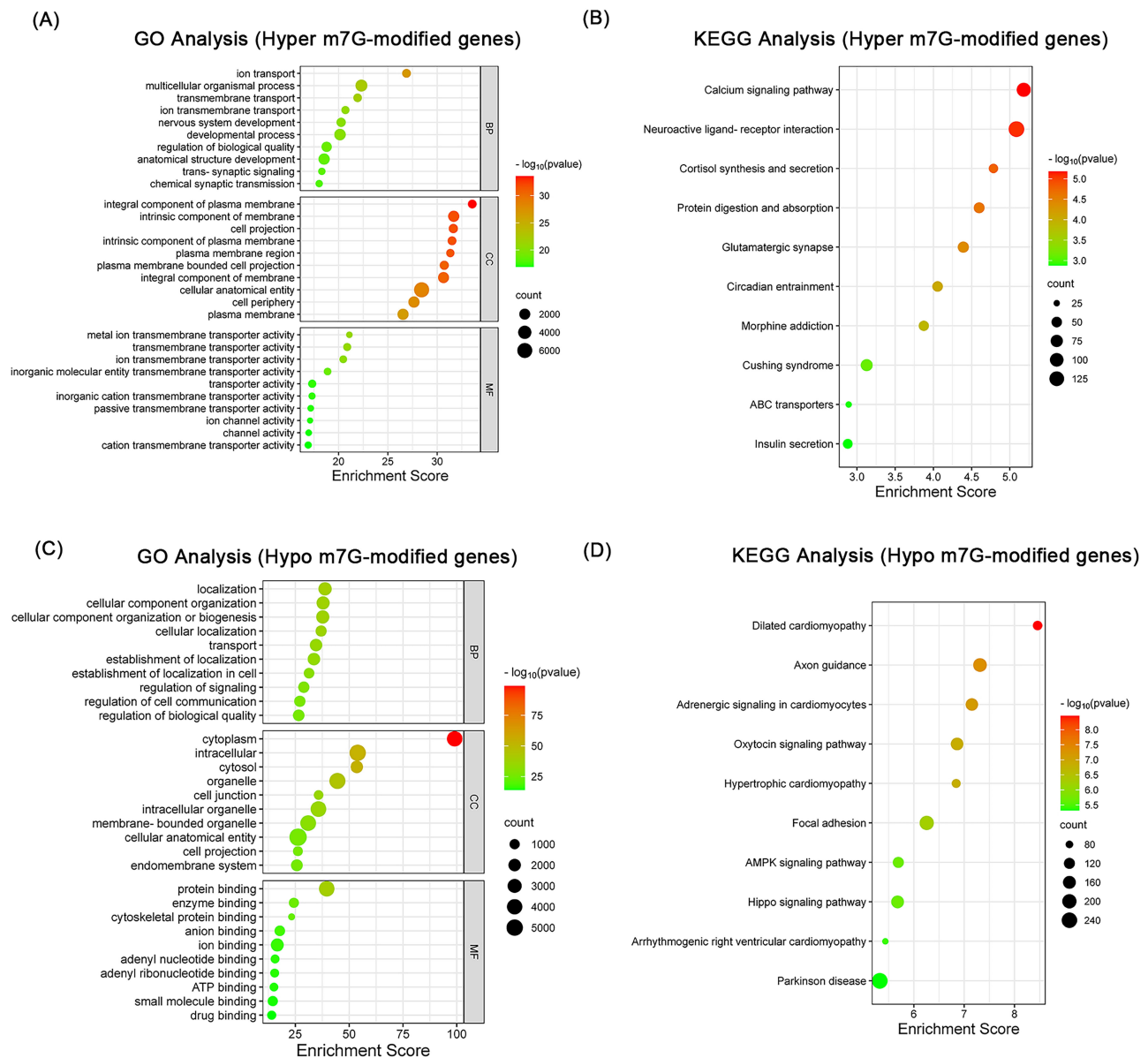


Fig. 2. The bioinformatic function of differentially methylated genes in OSCC. The top 10 Gene Ontology (GO) terms (A) and Kyoto Encyclopedia of Genes and Genomes (KEGG) pathways (B) of hyper m7G-modified genes in OSCC. GO enrichment included biological process (BP), cellular component (CC) and molecular function (MF). The top 10 GO terms (C) and KEGG pathways (D) of hypo m7G-modified genes in OSCC. Enrichment score: $-\log_{10}(p)$; Size: gene count.

[35]. Additionally, previous studies have found that m7G methylation usually acts through methyltransferases, and the methyltransferases that have been identified and studied include methyltransferase-like1 (METTL1), WD repeat domain 4 (WDR4), Williams Beuren syndrome chromosome region 22 (WBSCR22) and RNA guanine-7 methyltransferase (RNMT) [35,36]. The METTL1/WDR4 complex, identified as an m7G methyltransferase of tRNAs, may influence the metabolic process of RNA, which affects the progression of tumors [14]. A recent study reported that m7G-modified tRNA catalyzed by the METTL1/WDR4 complex could stabilize tRNAs, enhancing the transla-

tion of oncogenic genes in HNSCC [14]. Importantly, METTL1 has been revealed to be a methyltransferase that installs a subset of m7G into mRNAs [11]. Whether the METTL1/WDR4 complex in OSCC can affect the gene expression by mediating their internal m7G methylation levels needs to be further explored.

To explore the role of m7G methylation in diseases progression, researchers developed the MeRIP-seq technology based on specific m7G antibodies for transcriptional profiling of m7G methylation in human cells or tissues [11,13,37]. Likewise, to understand the status of m7G methylation in OSCC, the m7G MeRIP-seq method was

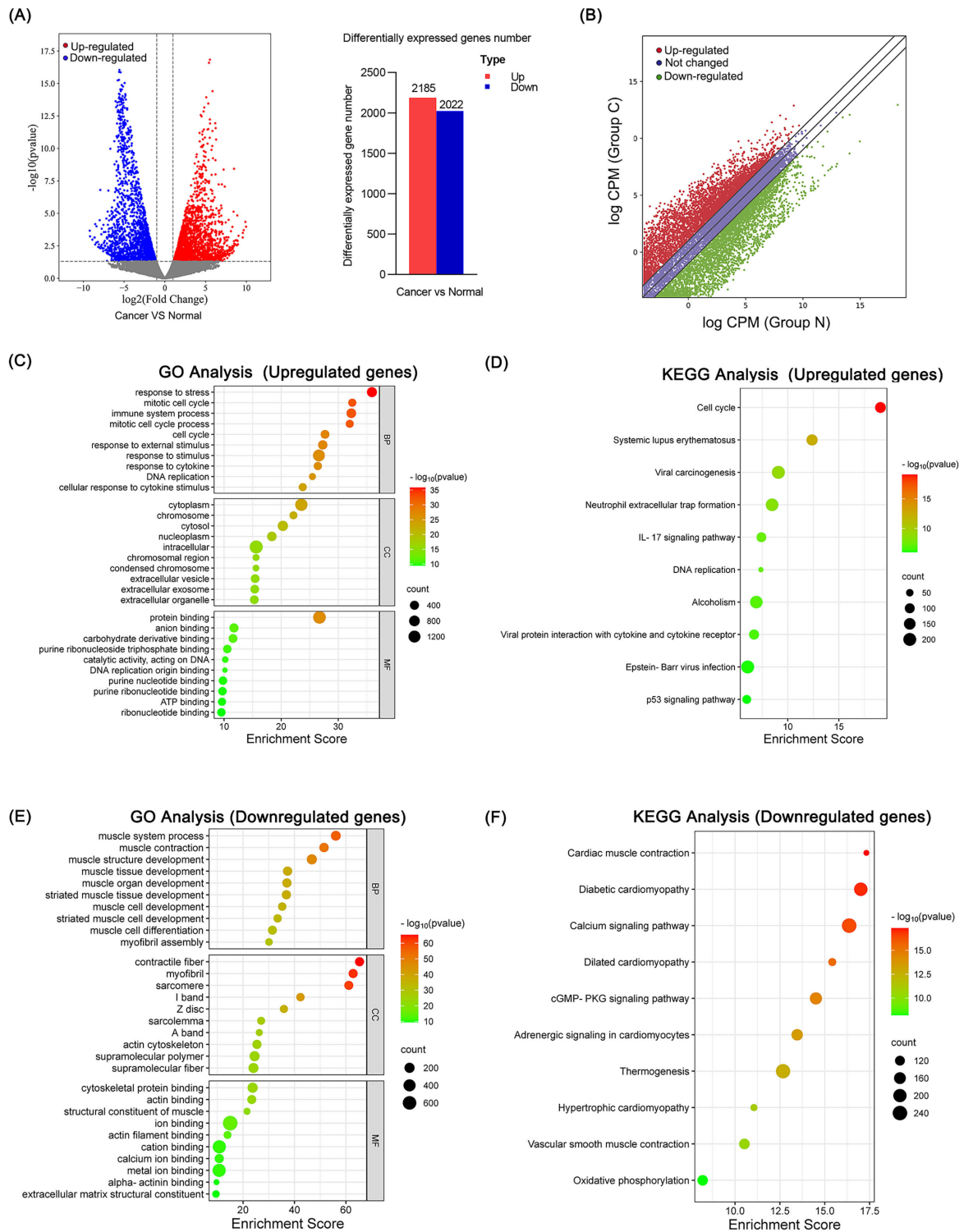


Fig. 3. The bioinformatic function was analyzed for differentially expressed genes identified in OSCC. (A) The volcano map showed differentially expressed genes in OSCC. The bar chart showed statistic of differential expressed genes between OSCC and normal tissues. (red: upregulated, grey: not changed, blue: downregulated). (B) Scatter plot showed differentially expressed genes. (Red: upregulated, Blue: not changed, Green: downregulated; C: cancer; N: normal). The top 10 GO terms (C) and KEGG pathways (D) of upregulated genes in OSCC. The top 10 GO terms (E) and KEGG pathway (F) on downregulated genes in OSCC. Enrichment score: $-\log_{10}(p)$; Size: gene count.

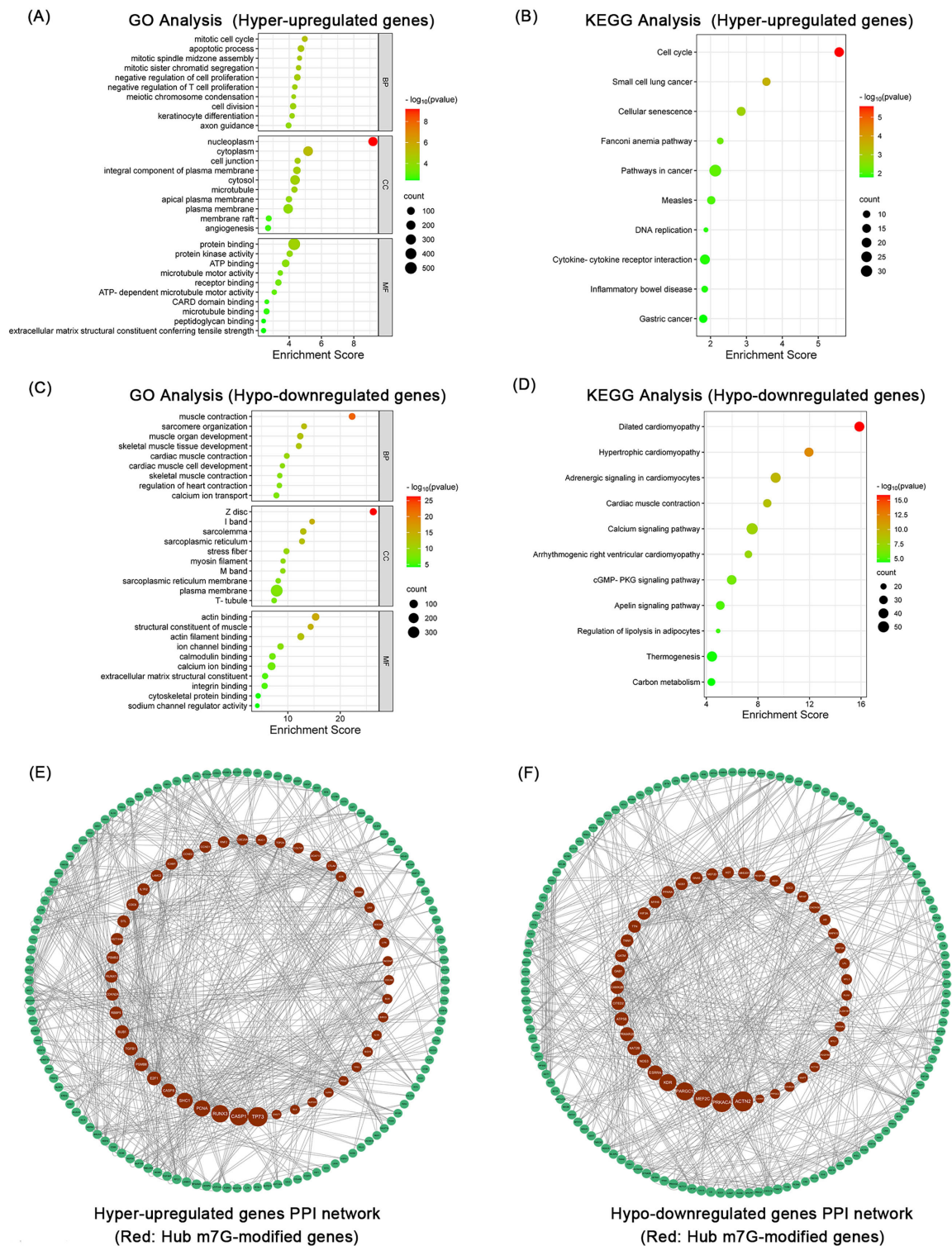


Fig. 4. Bioinformatics analysis of differentially expressed methylation genes identified by co-analysis. The top 10 GO terms (A) and KEGG pathways (B) of hyper-upregulated genes in OSCC. The top 10 GO terms (C) and KEGG pathways (D) of hypo-downregulated genes in OSCC. Enrichment score: $-\log_{10}(p)$; Size: gene count. (E) The protein-protein interaction (PPI) network was constructed among 1221 hyper-upregulated genes, and *TP73*, *CASP1* and *RUNX3* were identified as hub genes. (F) The PPI network was constructed among 1645 hypo-downregulated genes, and *ACTN2*, *PPKACA* and *MEF2C* were identified as hub genes. The red circles represent the screened hub genes.

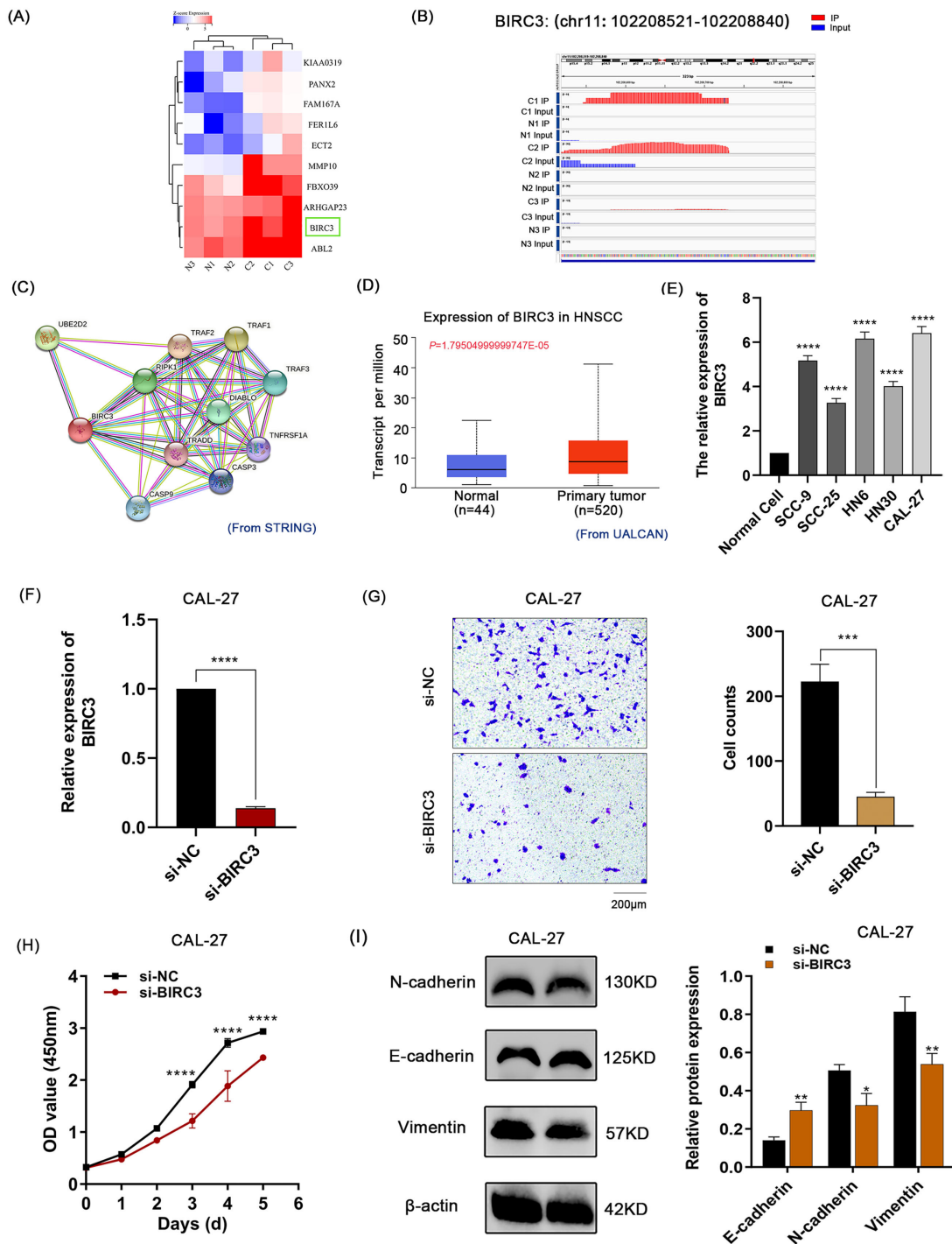


Fig. 5. The Bioinformatic characterization and biological functions of the *BIRC3* gene in OSCC. (A) The heatmap showed the top 10 upregulated genes with hypermethylation sites. (B) Visualization of the m7G peak site (chr11:102208521-102208840) in the *BIRC3* gene in OSCC tissues. (IP: immunoprecipitation; Red: IP; Blue: Input). (C) The PPI network of *BIRC3* was constructed by the STRING software. (D) Gene differential expression analysis from UALCAN showed that the mRNA expression of *BIRC3* was significantly upregulated in HNSCC tissues. (E) The high expression of *BIRC3* in OSCC cell lines was verified by qPCR assay. (F) The knockdown of *BIRC3* at the mRNA level in CAL-27 cells was confirmed by qPCR assay. (G) The Transwell migration assay showed the migration of CAL-27 cells transfected with si-BIRC3 was significantly inhibited. (H) The proliferation ability of CAL-27 transfected with si-BIRC3 was significantly reduced in the CCK-8 assay. OD, optical density. (I) The relative expression of EMT marker protein E-cadherin was significantly increased in the CAL-27 cells transfected with si-BIRC3, while the N-cadherin and Vimentin proteins were significantly decreased using Western blot assay. (*: $p < 0.05$, **: $p < 0.01$, ***: $p < 0.001$, ****: $p < 0.0001$).

used to measure the internal m7G methylated levels of mRNAs in OSCC and normal tissue in this study. However, m7G MeRIP-seq method still has limitations in detecting the internal mRNAs, which might result in the minor overlap in m7G peaks [11,38]. This result revealed the difference in m7G methylation between OSCC and normal tissue, suggesting that m7G methylation might be associated with the progress of OSCC. Importantly, the mechanism by which m7G regulates gene expression was closely related to the distribution region of m7G methylation within mRNAs [39]. It was found that gene expression was closely associated with elevated levels of m7G methylation in the CDS region, which might promote mRNA translation efficiency and protein expression [40]. Interestingly, it showed that m7G methylation was mainly enriched in the CDS region in OSCC tissues. Notably, the results also showed that there were more m7G peaks in the 5'UTR region of gene transcripts in OSCC tissues than in normal tissues, which might lead to abnormalities in various cellular interactions. For example, elevated m7G methylation in the 5'UTR region that assesses for complementarity with AUG might affect mRNA translational initiation, affecting critical cancer-related gene expression [41]. The sequencing analysis showed the distribution ratio of internal m7G methylation in the region of mRNAs, which provides the theoretical basis for further investigating the pathogenic mechanism of m7G methylation in OSCC.

The Bioinformatics function analysis showed that differentially methylated genes were associated with ABC transporters and the AMPK signaling pathway in OSCC tissues. Significantly, these cellular biological functions are associated with cancer progression. OSCC patients often develop multidrug resistance during clinical treatment, which significantly reduces the efficacy [42]. Previous studies have shown that high expression of ABC transporter (ABCC1 and ABCG2) promotes multidrug resistance in OSCC [42]. Moreover, the AMPK signaling pathway could participate in the proliferation migration in OSCC [43] and is critical in tumor metabolism [44]. We hypothesize that hypo m7G-modified genes in OSCC tissues might lead to abnormalities in tumor metabolism, which would be related to cancer progression. Thus, many cellular biological functions of these differentially methylated genes may provide clues to further clarify further the specific role of m7G methylation in OSCC.

This study showed the correlation between mRNA expression and m7G methylation, and 1221 hyper-upregulated genes and 1645 hypo-downregulated genes were identified. The hub genes *TP73*, *CASPI*, *RUNX3*, *ACTN2*, *PPKACA* and *MEF2C* were screened from the PPI network constructed for these genes. Previous studies demonstrated these hub genes could affect tumor development [45–47]. For example, *TP73* is highly expressed in OSCC and can influence cell biological processes of tumorigenesis, such as apoptosis, autophagy and

metabolism in tumors [45,46]. The downregulated expression of *ACTN2* in OSCC is associated with increased survival [47]. However, these genes' RNA methylation and regulatory roles have been poorly studied. Therefore, the m7G-modified hub genes provides significant value for studying the specific regulatory mechanisms of m7G methylation in OSCC. Notably, we screened the essential m7G-modified gene *BIRC3* by co-analysis.

BIRC3 is a member of the inhibitors of apoptosis proteins (IAPs) family, which can be involved in cellular bioprocesses through the regulation of cysteine asparaginase and the signaling of mitotic kinases [48]. Notably, the highly expressed *BIRC3* is significantly correlated with poor prognosis and chemotherapy resistance among multiple cancers, including non-small cell lung cancer [49], esophageal squamous cell carcinoma [50], HNSCC [51], and colorectal cancer [52]. Previous studies have reported that the *BIRC3* gene can act as an oncogenic factor in HNSCC [51]. Our sequencing results showed that the highly expressed *BIRC3* gene had high m7G methylation, and it was identified that the expression of *BIRC3* was higher in OSCC cell lines than in normal cells, consistent with the sequencing results. Furthermore, high-expressed *BIRC3* in OSCC was associated with poor prognosis, lymph node metastasis, and radiotherapy resistance [53,54]. The expression of *BIRC3* up-regulated by circDOCK1 was found to inhibit OSCC cell apoptosis [55]. In this study, the function of *BIRC3* with high m7G methylation in OSCC was also explored. *BIRC3* could promote the ability of proliferation and migration and the progress of EMT. Previous studies found that the Snail transcription factor could interact with *BIRC3*, thus promoting ovarian carcinogenesis [56]. The mechanisms by which *BIRC3* affects EMT progression need further investigation.

5. Conclusions

The m7G methylation difference in internal mRNAs between OSCC and normal tissues were analyzed. GO and KEGG pathway analyses revealed that m7G-modified genes were closely associated with cancer progression. Furthermore, *BIRC3* could promote the biological behavior of OSCC *in vitro*, which may be related to the process of EMT. This article identified critical m7G-modified genes and investigated their potential functions, providing a foundation for further research on the role of m7G methylation in OSCC.

Abbreviations

OSCC, Oral squamous cell carcinoma; MeRIP, Methylated RNA immunoprecipitation; m7G, N7-methylguanosine; rRNA, Ribosomal RNA; tRNA, Transfer RNA; miRNA, MicroRNA; CDS, Coding Sequence; GO, Gene Ontology; KEGG, Kyoto Encyclopedia of Genes and Genomes; DAVID, Database for Annotation, Visualization and Integrated Discovery; TIMER, Tumor

Immune Estimation Resource; UALCAN, University of Alabama at Birmingham Cancer Data Analysis Portal; GEPIA, Gene Expression Profiling Interactive Analysis; PPI, protein-protein interaction; STRING, Search Tool for Retrieval of Interacting Genes/Proteins software; DMEM, Dulbecco's Modified Eagle's Medium; FBS, fetal bovine serum; siRNA, Small interfering RNA; qPCR, quantitative real-time PCR; CCK-8, Cell Counting Kit-8; OD, optical density; IP, Immunoprecipitation; BP, biological processes; CC, cellular component; MF, molecular function; ABC transporters, ATP-binding cassette transporters; BIRC3, Baculoviral IAP Repeat Containing 3; AML, Acute Myeloid Leukemia; HNSCC, Head and neck squamous Cell carcinoma; METTL1, Methyltransferase-like 1; WDR4, WD repeat domain 4; RNMT, RNA guanine-7 methyltransferase; WBSR22, Williams Beuren syndrome chromosome region 22; UTR, Untranslated Region; AMPK, Adenosine 5 monophosphate (AMP)-activated protein kinase; EMT, epithelial-mesenchymal transition; m6A, N6-methyladenosine; Igv, Integrative Genomics Viewer; lncRNA, long noncoding RNA.

Availability of Data and Materials

Data supporting the findings of this study are available within the paper and its Supplemental information files. The datasets presented in this study have been deposited in the NCBI GEO database [17].

Author Contributions

YJ designed the research. ML, NS and DS contributed to acquisition and analysis of data and drafting the manuscript. YY and WZ performed the data analysis. XZ and MX performed the statistical analysis. JY and RS participated in image organization and data analysis. TG contributed to the writing and cellular experiments. All authors contributed to editorial changes in the manuscript. All authors read and approved the final manuscript. All authors have participated sufficiently in the work and agreed to be accountable for all aspects of the work.

Ethics Approval and Consent to Participate

Tissue samples for research were collected in accordance with the Declaration of Helsinki and was approved by the Ethics Committee of Weifang Medical University (ethics number: 2022YX007). The informed consent was obtained from all patients.

Acknowledgment

We thank all subjects who participated in this study. We thank Cloud-Seq Biotech Ltd. Co. (Shanghai, China) for the MeRIP-Seq service.

Funding

This study was supported by grants from the National Natural Science Foundation of China (82103008), Shandong Provincial Natural Science Foundation (ZR2023LSW019, ZR2020MH192, ZR2022QH122), 2021 Youth Innovation Talent Introduction and Education Program of Shandong Province Universities (for YYJ), National College Students Innovation and Entrepreneurship Training Program (202310438050), Shandong Provincial College Students Innovation and Entrepreneurship Training Program (S202310438051), the College students Innovation and Entrepreneurship Training program of Weifang Medical University (X2023050, X2023051, X2023376), and the National Facility for Translational Medicine (Shanghai) (TMSF-2021-2-003).

Conflict of Interest

The authors declare no conflict of interest.

Supplementary Material

Supplementary material associated with this article can be found, in the online version, at <https://doi.org/10.31083/j.fbl2812330>.

References

- [1] Siegel RL, Miller KD, Wagie NS, Jemal A. Cancer statistics, 2023. *CA: a Cancer Journal for Clinicians*. 2023; 73: 17–48.
- [2] Hedberg ML, Goh G, Chiosea SI, Bauman JE, Freilino ML, Zeng Y, *et al.* Genetic landscape of metastatic and recurrent head and neck squamous cell carcinoma. *Journal of Clinical Investigation*. 2016; 126: 1606–1606.
- [3] Sung H, Ferlay J, Siegel RL, Laversanne M, Soerjomataram I, Jemal A, *et al.* Global Cancer Statistics 2020: GLOBOCAN Estimates of Incidence and Mortality Worldwide for 36 Cancers in 185 Countries. *CA: a Cancer Journal for Clinicians*. 2021; 71: 209–249.
- [4] Gharat SA, Momin M, Bhavsar C. Oral Squamous Cell Carcinoma: Current Treatment Strategies and Nanotechnology-Based Approaches for Prevention and Therapy. *Critical Reviews™ in Therapeutic Drug Carrier Systems*. 2016; 33: 363–400.
- [5] Yi C, Pan T. Cellular Dynamics of RNA Modification. *Accounts of Chemical Research*. 2011; 44: 1380–1388.
- [6] You X, Yuan B. Detecting Internal N7-Methylguanosine mRNA Modifications by Differential Enzymatic Digestion Coupled with Mass Spectrometry Analysis. *Methods in Molecular Biology*. 2021; 23: 247–259.
- [7] Sloan KE, Warda AS, Sharma S, Entian K, Lafontaine DLJ, Bohnsack MT. Tuning the ribosome: the influence of rRNA modification on eukaryotic ribosome biogenesis and function. *RNA Biology*. 2017; 14: 1138–1152.
- [8] Guy MP, Phizicky EM. Two-subunit enzymes involved in eukaryotic post-transcriptional tRNA modification. *RNA Biology*. 2014; 11: 1608–1618.
- [9] Pandolfini L, Barbieri I, Bannister AJ, Hendrick A, Andrews B, Webster N, *et al.* METTL1 Promotes let-7 MicroRNA Processing via m7G Methylation. *Molecular Cell*. 2019; 74: 1278–1290.e9.
- [10] Yang S, Zhou J, Chen Z, Sun Q, Zhang D, Feng Y, *et al.* A novel m7G-related lncRNA risk model for predicting prognosis and

- evaluating the tumor immune microenvironment in colon carcinoma. *Frontiers in oncology*. 2022; 12: 934928.
- [11] Zhang L, Liu C, Ma H, Dai Q, Sun H, Luo G, *et al.* Transcriptome-wide Mapping of Internal N7-Methylguanosine Methylome in Mammalian mRNA. *Molecular Cell*. 2019; 74: 1304–1316.e8.
- [12] Zhao Y, Kong L, Pei Z, Li F, Li C, Sun X, *et al.* m7G Methyltransferase METTL1 Promotes Post-ischemic Angiogenesis via Promoting VEGFA mRNA Translation. *Frontiers in cell and developmental biology*. 2021; 9: 642080.
- [13] Zhang B, Li D, Wang R. Transcriptome Profiling of N7-Methylguanosine Modification of Messenger RNA in Drug-Resistant Acute Myeloid Leukemia. *Frontiers in oncology*. 2022; 12: 926296.
- [14] Chen J, Li K, Chen J, Wang X, Ling R, Cheng M, *et al.* Aberrant translation regulated by METTL1/WDR4-mediated tRNA N7-methylguanosine modification drives head and neck squamous cell carcinoma progression. *Cancer Communications*. 2022; 42: 223–244.
- [15] Chen B, Jiang W, Huang Y, Zhang J, Yu P, Wu L, *et al.* N7-methylguanosine tRNA modification promotes tumorigenesis and chemoresistance through WNT/ β -catenin pathway in nasopharyngeal carcinoma. *Oncogene*. 2022; 41: 2239–2253.
- [16] Huang G, Wu Q, Zheng Z, Shao T, Chen Y, Zeng W, *et al.* M6a-related bioinformatics analysis reveals that HNRNPC facilitates progression of OSCC via EMT. *Aging*. 2020; 12: 11667–11684.
- [17] Sun D, Song N, Li M, Chen X, Zhang X, Yu Y, *et al.* Comprehensive analysis of circRNAs for N7-methylguanosine methylation modification in human oral squamous cell carcinoma. *FASEB BioAdvances*. 2023; 5: 305–320.
- [18] Kechin A, Boyarskikh U, Kel A, Filipenko M. CutPrimers: a New Tool for Accurate Cutting of Primers from Reads of Targeted next Generation Sequencing. *Journal of Computational Biology*. 2017; 24: 1138–1143.
- [19] Kim D, Langmead B, Salzberg SL. HISAT: a fast spliced aligner with low memory requirements. *Nature Methods*. 2015; 12: 357–360.
- [20] Robinson MD, McCarthy DJ, Smyth GK. edgeR: a Bioconductor package for differential expression analysis of digital gene expression data. *Bioinformatics*. 2010; 26: 139–140.
- [21] Zhang Y, Liu T, Meyer CA, Eeckhoute J, Johnson DS, Bernstein BE, *et al.* Model-based Analysis of ChIP-Seq (MACS) *Genome Biology*. 2008; 9: R137.
- [22] Shen L, Shao NY, Liu X, Maze I, Feng J, Nestler EJ. diffReps: detecting differential chromatin modification sites from ChIP-seq data with biological replicates. *PLoS ONE*. 2013; 8: e65598.
- [23] Zhang H, Meltzer P, Davis S. RCircos: an R package for Circos 2D track plots. *BMC Bioinformatics*. 2013; 14: 244.
- [24] Bailey TL. STREME: accurate and versatile sequence motif discovery. *Bioinformatics*. 2021; 37: 2834–2840.
- [25] Dennis G, Sherman BT, Hosack DA, Yang J, Gao W, Lane HC, *et al.* DAVID: Database for Annotation, Visualization, and Integrated Discovery. *Genome Biology*. 2003; 4: P3.
- [26] Szklarczyk D, Gable AL, Nastou KC, Lyon D, Kirsch R, Pyysalo S, *et al.* The STRING database in 2021: customizable protein–protein networks, and functional characterization of user-uploaded gene/measurement sets. *Nucleic Acids Research*. 2021; 49: D605–D612.
- [27] Tang Y, Li M, Wang J, Pan Y, Wu F. CytoNCA: a cytoscape plugin for centrality analysis and evaluation of protein interaction networks. *Biosystems*. 2015; 127: 67–72.
- [28] Li T, Fu J, Zeng Z, Cohen D, Li J, Chen Q, *et al.* TIMER2.0 for analysis of tumor-infiltrating immune cells. *Nucleic Acids Research*. 2020; 48: W509–W514.
- [29] Chandrashekar DS, Karthikeyan SK, Korla PK, Patel H, Shovon AR, Athar M, *et al.* UALCAN: an update to the integrated cancer data analysis platform. *Neoplasia*. 2022; 25: 18–27.
- [30] Tang Z, Li C, Kang B, Gao G, Li C, Zhang Z. GEPIA: a web server for cancer and normal gene expression profiling and interactive analyses. *Nucleic Acids Research*. 2017; 45: 98–102.
- [31] Jiang Y, Cao W, Wu K, Qin X, Wang X, Li Y, *et al.* LncRNA LINC00460 promotes EMT in head and neck squamous cell carcinoma by facilitating peroxiredoxin-1 into the nucleus. *Journal of Experimental & Clinical Cancer Research*. 2019; 38: 365.
- [32] Chen X, Liu Y, Sun D, Sun R, Wang X, Li M, *et al.* Long non-coding RNA lnc-H2AFV-1 promotes cell growth by regulating aberrant m6A RNA modification in head and neck squamous cell carcinoma. *Cancer Science*. 2022; 113: 2071–2084.
- [33] Jiang Y, Guo H, Tong T, Xie F, Qin X, Wang X, *et al.* LncRNA lnc-POP1-1 upregulated by VN1R5 promotes cisplatin resistance in head and neck squamous cell carcinoma through interaction with MCM5. *Molecular Therapy*. 2022; 30: 448–467.
- [34] Gallo-Oller G, Ordoñez R, Dotor J. A new background subtraction method for Western blot densitometry and band quantification through image analysis software. *Journal of Immunological Methods*. 2018; 457: 1–5.
- [35] Luo Y, Yao Y, Wu P, Zi X, Sun N, He J. The potential role of N7-methylguanosine (m7G) in cancer. *Journal of Hematology & Oncology*. 2022; 15: 63.
- [36] Ying X, Liu B, Yuan Z, Huang Y, Chen C, Jiang X, *et al.* METTL1-m(7) G-EGFR/EFEMP1 axis promotes the bladder cancer development. *Clinical and Translational Medicine*. 2021; 11: e675.
- [37] Chen X, Li X, Xu S, Hu S, Wang T, Li R, *et al.* TMEM11 regulates cardiomyocyte proliferation and cardiac repair via METTL1-mediated m7G methylation of ATF5 mRNA. *Cell Death and Differentiation*. 2023; 30: 1786–1798.
- [38] Wang H, Chen RB, Zhang SN, Zhang RF. N7-methylguanosine modification of lncRNAs in a rat model of hypoxic pulmonary hypertension: a comprehensive analysis. *BMC Genomics*. 2022; 23: 33.
- [39] Meyer K, Saletore Y, Zumbo P, Elemento O, Mason C, Jaffrey S. Comprehensive Analysis of mRNA Methylation Reveals Enrichment in 3' UTRs and near Stop Codons. *Cell*. 2012; 149: 1635–1646.
- [40] Malbec L, Zhang T, Chen Y, Zhang Y, Sun B, Shi B, *et al.* Dynamic methylome of internal mRNA N7-methylguanosine and its regulatory role in translation. *Cell Research*. 2019; 29: 927–941.
- [41] Haimov O, Sinvani H, Dikstein R. Cap-dependent, scanning-free translation initiation mechanisms. *Biochimica Et Biophysica Acta (BBA) - Gene Regulatory Mechanisms*. 2015; 1849: 1313–1318.
- [42] Shang HG, Yu HL, Ma XN, Xu X. Multidrug resistance and tumor-initiating capacity of oral cancer stem cells. *Journal of B.U.ON. : official journal of the Balkan Union of Oncology*. 2016; 21: 461–465.
- [43] Bai G, Chen B, Xiao X, Li Y, Liu X, Zhao D, *et al.* Geniposide inhibits cell proliferation and migration in human oral squamous carcinoma cells via AMPK and JNK signaling pathways. *Experimental and Therapeutic Medicine*. 2022; 24: 706.
- [44] Zhao Y, Hu X, Liu Y, Dong S, Wen Z, He W, *et al.* ROS signaling under metabolic stress: cross-talk between AMPK and AKT pathway. *Molecular Cancer*. 2017; 16: 79.
- [45] Bidaud P, Chasle J, Sichel F, Rousseau S, Petit P, Pottier D, *et al.* Expression of p53 family members and CD44 in oral squamous cell carcinoma (OSCC) in relation to tumorigenesis. *Histology and Histopathology*. 2010; 25: 331–339.
- [46] Nemerova A, Amelio I, Gebel J, Dötsch V, Melino G, Moll UM. Non-oncogenic roles of Tap73: from multiciliogenesis to metabolism. *Cell Death and Differentiation*. 2018; 25: 144–153.
- [47] Dai Y, Lv Q, Qi T, Qu J, Ni H, Liao Y, *et al.* Identification of hub

- methyated-CpG sites and associated genes in oral squamous cell carcinoma. *Cancer Medicine*. 2020; 9: 3174–3187.
- [48] Frazzi R. BIRC3 and BIRC5: multi-faceted inhibitors in cancer. *Cell & Bioscience*. 2021; 11: 8.
- [49] Liu C, Chen Z, Ding X, Qiao Y, Li B. Ubiquitin-specific protease 35 (USP35) mediates cisplatin-induced apoptosis by stabilizing BIRC3 in non-small cell lung cancer. *Laboratory Investigation*. 2022; 102: 524–533.
- [50] Wu Q, Zhang Y, An H, Sun W, Wang R, Liu M, *et al*. The landscape and biological relevance of aberrant alternative splicing events in esophageal squamous cell carcinoma. *Oncogene*. 2021; 40: 4184–4197.
- [51] Lee MK, Noh JK, Woo SR, Kong M, Lee YC, Lee JW, *et al*. Prognostic Significance of the BIRC2-BIRC3 Gene Signature in Head and Neck Squamous Cell Carcinoma. *Cancer Genomics & Proteomics*. 2022; 19: 591–605.
- [52] Zhang S, Yang Y, Weng W, Guo B, Cai G, Ma Y, *et al*. *Fusobacterium nucleatum* promotes chemoresistance to 5-fluorouracil by upregulation of BIRC3 expression in colorectal cancer. *Journal of Experimental & Clinical Cancer Research: CR*. 2019; 38: 14.
- [53] Bhosale PG, Pandey M, Cristea S, Shah M, Patil A, Beerwinkeln N, *et al*. Recurring Amplification at 11q22.1-q22.2 Locus Plays an Important Role in Lymph Node Metastasis and Radioreistance in OSCC. *Scientific Reports*. 2017; 7: 16051.
- [54] Bhosale PG, Cristea S, Ambatipudi S, Desai RS, Kumar R, Patil A, *et al*. Chromosomal Alterations and Gene Expression Changes Associated with the Progression of Leukoplakia to Advanced Gingivobuccal Cancer. *Translational Oncology*. 2017; 10: 396–409.
- [55] Wang L, Wei Y, Yan Y, Wang H, Yang J, Zheng Z, *et al*. CircDOCK1 suppresses cell apoptosis via inhibition of miR-196a-5p by targeting BIRC3 in OSCC. *Oncology Reports*. 2018; 39: 951–966.
- [56] Rho SB, Byun H, Kim B, Lee CH. Snail Promotes Cancer Cell Proliferation via its Interaction with the BIRC3. *Biomolecules & Therapeutics*. 2022; 30: 380–388.